Volume 4 | Number 9 | September 2018 | Pages 1203–1378

Environmental Science
Water Research & Technology

rsc.li/es-water

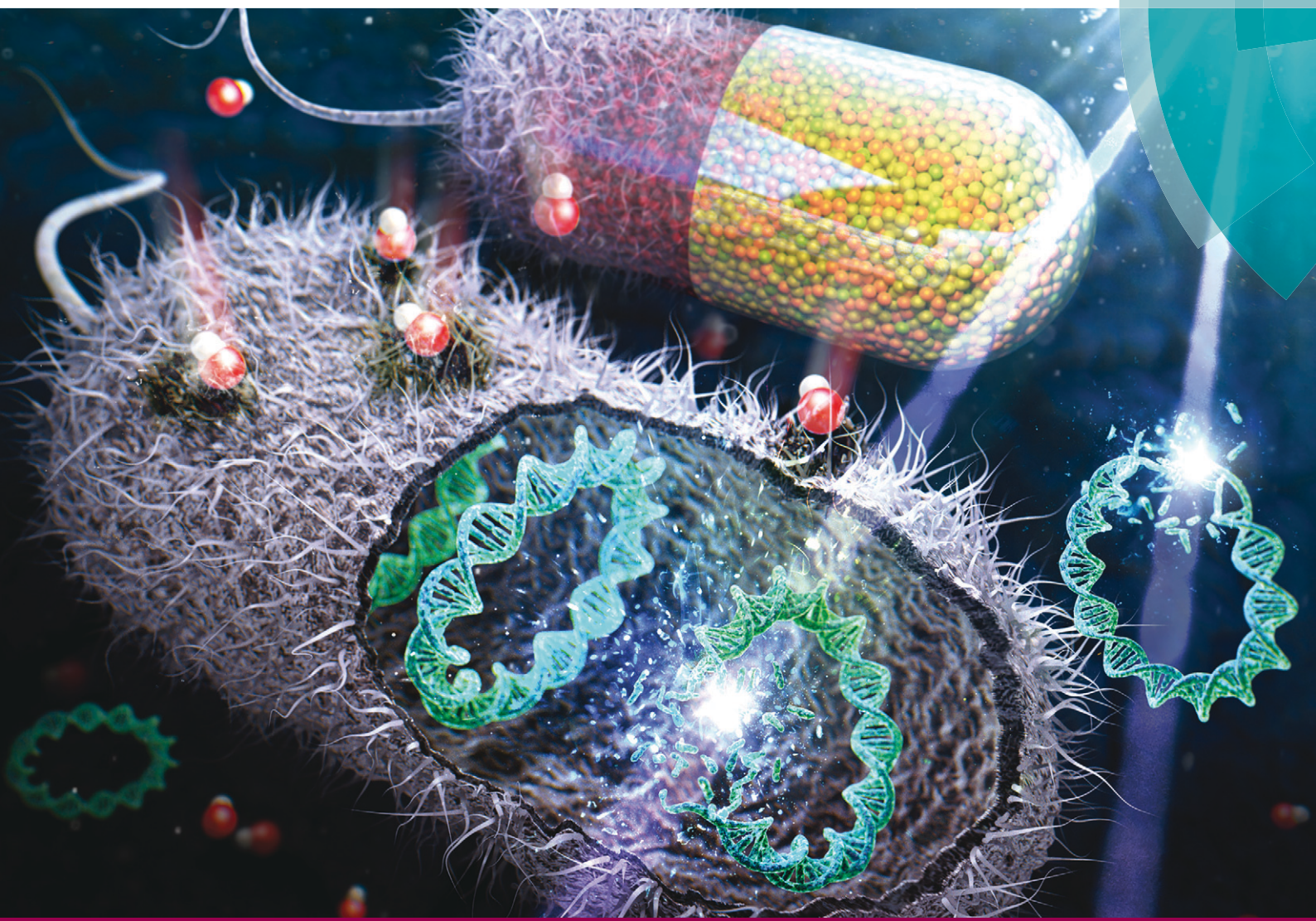

Themed issue: Ultraviolet-based Advanced Oxidation Processes (UV AOPs)

ISSN 2053-1400

ROYAL SOCIETY OF CHEMISTRY

PAPER
Yunho Lee *et al.*
Elimination of transforming activity and gene degradation during UV and UV/H_2O_2 treatment of plasmid-encoded antibiotic resistance genes

Environmental Science
Water Research & Technology

PAPER

View Article Online
View Journal | View Issue

Cite this: *Environ. Sci.: Water Res. Technol.*, 2018, **4**, 1239

Elimination of transforming activity and gene degradation during UV and UV/H_2O_2 treatment of plasmid-encoded antibiotic resistance genes†

Younggun Yoon,[a] Michael C. Dodd[b] and Yunho Lee *[a]

Received 31st March 2018,
Accepted 29th May 2018

DOI: 10.1039/c8ew00200b

rsc.li/es-water

To better understand the elimination of transforming activity of antibiotic resistance genes (ARGs), this study investigated the deactivation of transforming activity of an ARG (in *Escherichia coli* as a host) and ARG degradation (according to quantitative PCR [qPCR] with different amplicon sizes) during UV (254 nm) and UV/H_2O_2 treatments of plasmid pUC19 containing an ampicillin resistance gene (*amp*^{R}). The required UV fluence for each $\log_{10}$ reduction of the transforming activity during UV treatment was ~37 mJ cm^{-2} for both extra- and intra-cellular pUC19 (the latter within *E. coli*). The resulting fluence-based rate constant (*k*) of ~6.2 × 10^{-2} cm^2 mJ^{-1} was comparable to the *k* determined previously for transforming activity loss of plasmids using host cells capable of DNA repair, but much lower (~10-fold) than that for DNA repair-deficient cells. The *k* value for pUC19 transforming activity loss was similarly much lower than the *k* calculated for cyclobutane-pyrimidine dimer (CPD) formation in the entire plasmid. These results indicate the significant role of CPD repair in the host cells. The degradation rate constants (*k*) of *amp*^{R} measured by qPCR increased with increasing target amplicon size (192–851 bp) and were close to the *k* calculated for the CPD formation in the given amplicons. Further analysis of the degradation kinetics of plasmid-encoded genes from this study and from the literature revealed that qPCR detected most UV-induced DNA damage. In the extracellular plasmid, DNA damage mechanisms other than CPD formation (*e.g.*, base oxidation) were detectable by qPCR and gel electrophoresis, especially during UV/H_2O_2 treatment. Nevertheless, the enhanced DNA damage for the extracellular plasmids did not result in faster elimination of the transforming activity. Our results indicate that calculated CPD formation rates and qPCR analyses are useful for predicting and/or measuring the rate of DNA damage and predicting the efficiency of transforming activity elimination for plasmid-encoded ARGs during UV-based water disinfection and oxidation processes.

Water impact

The efficiency and mode of action for deactivating and degrading antibiotic resistance genes (ARGs) during water treatment with UV (254 nm) and UV/H_2O_2 have been poorly understood. Here, we show that the efficiency of elimination of the transforming activity for a plasmid-encoded ARG during the UV-based treatments depends on the rate of formation of cyclobutane-pyrimidine dimers (CPDs) in the plasmid and the repair of such DNA damage during the transformation process in host cells. This work has important implications for optimizing the monitoring and operation of UV-based water disinfection and oxidation processes for removing ARGs.

Introduction

Increasing antibiotic resistance is a major threat to human and animal health, as it can lower the therapeutic potential of antibiotics against bacterial infections.[1] Although antibiotic resistance can occur naturally, overuse or misuse of antibiotics in modern society is associated with increased antibiotic resistance.[2] Antibiotics can select antibiotic-resistant bacteria (ARB) that carry genes (ARGs) responsible for antibiotic resistance mechanisms. The presence of ARB and ARGs in aquatic environments is a concern because it can promote the spread of antibiotic resistance through natural and anthropogenic water cycles.[3,4] In addition, antibiotic resistance can be disseminated among bacterial populations by sharing (mobile) ARGs through horizontal gene transfer (HGT) processes.[5] To minimize dissemination of environmental sources of antibiotic resistance, the necessity for coordinated

[a] *School of Earth Sciences and Environmental Engineering, Gwangju Institute of Science and Technology (GIST), Gwangju 61005, Republic of Korea. E-mail: yhlee42@gist.ac.kr; Fax: +82 62 715 2434; Tel: +82 62 715 2468*
[b] *Department of Civil and Environmental Engineering, University of Washington, Seattle, WA 98195, USA*

† Electronic supplementary information (ESI) available. See DOI: 10.1039/c8ew00200b

national and international strategies has been advised for monitoring, risk assessment, and mitigation of antibiotic resistance.[6]

Municipal wastewater has been identified as one of the hotspots that release ARB and ARGs into aquatic environments.[7,8] Conventional wastewater treatment does not fully eliminate ARB and ARGs.[7,9] Biological treatment processes (*e.g.*, activated sludge) can significantly reduce the load of ARB but may select highly (or multi-) resistant bacterial species.[10] Disinfection of wastewater effluents with chlorine or ultraviolet irradiation (UV) has been widely practiced for water resource protection.[11] Ozonation has recently received renewed attention as an option for treating municipal wastewater effluents to eliminate organic micropollutants.[12] Advanced oxidation processes such as UV/H_2O_2 treatment have also been tested to achieve the same goal.[13,14] There has been growing interest in the efficiency of wastewater disinfection and oxidation processes to lower the levels of ARB and ARGs, in addition to micropollutant elimination.[10,15–23]

ARGs in wastewaters exist in different forms such as intracellular (within bacteria) and extracellular, as free DNA and viruses.[24,25] ARGs can transfer resistance by HGT mechanisms such as conjugation, transduction, and transformation. Among these HGT mechanisms, transformation requires only intact ARGs for the resistance transfer, as extracellular ARGs can be taken up and incorporated into the genomes of competent bacteria even in the absence of the original donor ARB cell.[5] This mechanism is therefore different from conjugation or transduction in which viable donor cells or infective viruses containing ARGs are needed. Considering the potential for ARG transfer *via* transformation, it is necessary to assess the efficiency of disinfectants at destroying ARGs and eliminating their associated transforming activities.[16]

Molecular mechanisms of DNA damage induced by UV or by hydroxyl radicals (˙OH) are well established. UV (particularly UVC) mainly generates DNA base lesions such as cyclobutane-pyrimidine dimers (CPDs) and pyrimidine (6-4) pyrimidone adducts [(6-4) photoproducts].[26,27] Good correlations have been found between the UV-induced degradation rate of ARGs and the number of adjacent pyrimidine dimer sites.[19,28,29] Genomic modeling, an approach to predict the UV sensitivity of microorganisms based on their DNA sequence characteristics, has been tested to predict the degradation efficiency of ARGs.[29] For ˙OH, the DNA damage can range from base oxidation to sugar backbone breakages, where the latter can lead to single strand (ss) and double strand (ds) breaks.[30] Despite this knowledge, it is unclear how different types of DNA damage resulting from reactions with disinfectants (*e.g.*, UV, ˙OH) are related to the loss of ARG transforming activity.

Quantitative polymerase chain reaction (qPCR) has been widely used to detect and quantify ARGs present in aquatic environments.[31] The qPCR method has also been employed to assess the efficacy of disinfection processes for ARG elimination by quantifying target qPCR amplicons.[10,15,17–22,29] Most qPCR methods involve amplicons covering only portions of ARGs (*e.g.*, 100–200 bp) and rarely cover the entire genes that are necessary for gene transfer pathways.[19,22,28] In addition, the sensitivity of qPCR and bacterial gene transformation to DNA damage can differ due to the different degrees of DNA repair or DNA polymerase fidelity rates of qPCR *vs.* the bacterial cell system.[28] As an alternative approach, the transforming activity of ARGs can be directly measured by transformation assays in which the target ARG-containing DNA (*e.g.*, plasmid) is taken up by and incorporated into the genomes of nonresistant, competent bacterial cells.[16,31] Nevertheless, a few studies have applied such an ARG transformation assay to assess the efficacy of disinfection processes for the elimination of antibiotic resistance.[28] Furthermore, the relationship between the qPCR method and the transformation assay for determining a biologically active ARG concentration is still poorly understood.

To elucidate the efficiency of deactivation and degradation of ARGs during water disinfection and oxidation processes, in this study, we determined and compared the changes in transforming activity and ARG concentrations during UV_{254nm} (hereafter UV) or UV/H_2O_2 treatment of plasmid-encoded ARGs in bench scale disinfection experiments. A quantitative transformation assay employing *Escherichia coli* as the recipient was conducted to determine the transforming activity of the target plasmid. ARG concentrations were determined by qPCR with different amplicon sizes to determine the DNA damage in different parts of the target plasmid. In addition, agarose gel electrophoresis was carried out to determine structural changes of the plasmid. Both extracellular and intracellular forms of plasmids were treated to test the effects of cellular components on the efficiency of ARG elimination. The results were evaluated with respect to factors affecting the efficiency of elimination of ARGs' transforming activities, for example, DNA repair, plasmid characteristics, the type of DNA damage, and sensitivity of DNA polymerase.

Materials and methods

Standards and reagents

All chemicals and solvents (mostly of ≥95% purity) were purchased from various commercial suppliers and used as received (SI-Text-1†). Chemical solutions were prepared with ultrapure water (≥18.2 MΩ cm) that was obtained by means of a Barnstead purification system (Thermo Fisher Scientific, USA). Glassware was washed with ultrapure water and autoclaved at 121 °C for 15 min prior to use.

Model bacterial strains and ARG-containing plasmid

E. coli DH5α hosting plasmid pUC19 served as the model ARB in this study.[32] Nonresistant *E. coli* DH5α was used as the recipient strain for the ARG transformation assay. The *E. coli* stocks were prepared at concentrations of ~10^9 colony-forming units (CFU) per ml according to the method described elsewhere.[22] Cells from the mid-exponential growth phase were used. Plasmid pUC19 (2686 bp) is an *E. coli* vector that carries an ampicillin resistance gene (*amp*^{R}; see Fig. S1

and Table S1† for gene information). Plasmids were extracted from *E. coli* stocks with the AccuPrep Nano-Plus Plasmid Extraction Kit.[33] Extracted plasmids were analyzed and quantified on a NanoDrop ND-2000 spectrophotometer (NanoDrop Products, Wilmington, USA). Plasmid concentrations in the extracted stock solutions (50 μL) were $\sim 10^{11}$ copies per μL (or 0.5–1 μg μL^{-1}). See SI-Text-2† for further details.

Determination of transforming activity of plasmid-encoded ARG

To quantify the ability of the pUC19 plasmid to transfer its antibiotic resistance, a transformation assay was conducted with nonresistant *E. coli* DH5α as the recipient strain.[34] Competent cells were prepared by treating *E. coli* DH5α with calcium chloride and glycerol as the chemical treatment method[35] and stored at −80 °C until use (see SI-Text-3† for details). One-hundred μL of the competent cells ($\sim 7 \times 10^8$ CFU ml^{-1}) was thawed and prepared in 1.5 mL tubes, and mixed with 5–10 μL of the plasmid samples. The resulting mixtures were placed on ice for 30 min incubation, then quickly transferred into a water bath at 42 °C for 45 s and placed back on ice for 2 min. After heat shock, the samples were mixed with 900 μL of Luria–Bertani (LB) broth and cultured in a shaking incubator (200 rpm) at 37 °C for 45 min. The incubated samples were serially diluted with LB broth and plated onto LB agar plates containing 50 mg L^{-1} ampicillin. The concentration of the transformants was determined by enumerating the ARB colonies on the plates after 24 hours of incubation in the dark at 37 °C. Finally, the transforming activity of the samples was calculated as the concentration of transformants from colonies in selective plates (with ampicillin) normalized to the concentration of *E. coli* cells from colonies in nonselective plates (without ampicillin) as presented in eqn (1). From the nonselective plates, typical concentrations of $\sim 7 \times 10^8$ CFU mL^{-1} *E. coli* cells were determined under the tested conditions.

$$\text{Transforming activity} = [\text{Transformants}]_{\text{selectiveplate}} \div [\textit{E. coli}\ \text{cells}]_{\text{nonselectiveplate}} \quad (1)$$

qPCR

Amplicons spanning variable-length segments of the amp^R gene (192, 400, 603, and 851 bp of the overall 861 bp length of amp^R) and *ori* region (190, 390, and 530 bp of the overall 589 bp length of *ori*) in the pUC19 plasmid (2686 bp) were quantified by means of qPCR (Fig. S1, Table S1†). Amplicon and primer sequences were determined from the pUC19 sequence retrieved from the NCBI GenBank database. Primers were designed using the NCBI Primer-BLAST tool (Table S2†). qPCR measurements were performed on a CFX96 Real-Time PCR detection system (Bio-Rad, Hercules, CA, USA) using SsoFast™ EvaGreen® supermixes (Bio-Rad). Standard curves were generated from 10-fold serial dilutions covering 5 orders of magnitude. Each 20 μL qPCR reaction consisted of 1 μL of 0.5 pmol forward and reverse primers (0.5 pmol μl^{-1}), 1 μL of a DNA sample, 10 μL of an EvaGreen® supermix, and 8 μL of autoclaved DNase-free water. The temperature profile of the PCR protocol included one cycle at 95 °C for 2 min, 30 cycles at 95 °C for 5 s, an annealing step at 55 °C for 60 s, and an extension step at 72 °C for 20 s, followed by a melt curve analysis from 65 °C to 95 °C. The same PCR protocol was used for all qPCR assays with different amplicons. Calibration curves for the target amplicons exhibited r^2 values of ≥0.98 for all cases (Fig. S2† shows a representative example). The average amplification efficiencies for the amp^R amplicons were 0.90(±0.04) for 192 bp, 0.89(±0.06) for 400 bp, 0.84(±0.09) for 603 bp, and 0.88(±0.08) for the 851 bp amplicon. The average amplification efficiencies for the *ori* amplicons were 0.84(±0.05) for 190 bp, 0.95(±0.03) for 390 bp, and 0.93(±0.07) for the 530 bp amplicon. The limit of detection (LOD) and quantification (LOQ) were determined as 15 copies and 40 copies per reaction for most qPCR runs. The end products of qPCR analyses were also analyzed by agarose gel electrophoresis (Fig. S3†) to confirm successful amplification of the target genes. The samples from UV treatment were directly analyzed by the qPCR protocol described above for extracellular plasmids. For intracellular plasmids, 10 mL of a given sample containing disinfectant-treated or untreated *E. coli* DH5α cells was centrifuged, and the pellet was resuspended in 100 μL of Tris-HCl buffer (10 mM, pH 8.5). The resulting concentrated samples were processed with the AccuPrep Nano-Plus Plasmid Extraction Kit[33] and subsequently analyzed by the above qPCR protocol.

Gel electrophoresis

Samples were prepared by treating the extracted pUC19 (~5 μg mL^{-1}) at pH 7 (2 mM phosphate buffered solutions) with UV and UV/H_2O_2 at different UV fluence levels (0–312 mJ cm^{-2}). Linearized pUC19 plasmids were prepared by incubating the extracted pUC19 with type II restriction enzyme *EcoRI* (NEB, USA) at 37 °C for 1 h, followed by enzyme inactivation at 65 °C for 20 min. Standards of the amp^R amplicons with different sizes (192, 400, 603, and 851 bp) were prepared by qPCR reactions above. These prepared plasmid samples and a 1 kb DNA ladder (Enzynomics, KOREA) were loaded on 0.8% agarose gels containing 0.5 μg ml^{-1} ethidium bromide in 1× TAE (Tris-Acetate–EDTA) buffer and were separated at 4 V cm^{-1} for 35 min. Gel images were captured on a bench-top UV Transilluminator (Universal mutation detection system, UVP, LLC, USA). The density of each band on the gels was calculated by quantitative band analysis in the ImageJ software.[36] Isolated amp^R amplicons for the transforming activity determination were prepared by cutting the gels loaded with the amp^R qPCR amplicon mixtures and by subsequent purification with the AccuPrep® Gel Purification Kit (Bioneer).

UV and UV/H_2O_2 treatments

Bench scale UV irradiation experiments were conducted in a quasi-collimated beam system[37] equipped with a low-pressure mercury lamp emitting 254 nm light (Sankyo Denki

Ltd., Tokyo, Japan). The applied photon fluence rate was ~0.3 mW cm^{-2} as determined by a UVX digital radiometer (Ultra-Violet Products Ltd., Upland, USA) or by atrazine chemical actinometry.[38] Solutions of the pUC19 plasmid or *E. coli* were separately prepared in 2 mM phosphate buffer (pH 7) by adding the corresponding stock solutions at the concentration of ~10^{11} copies per mL for the plasmid or ~5×10^6 CFU mL^{-1} for *E. coli*, respectively. These samples (120 mL) were placed in a Petri dish reactor with a sample depth of 2.5 cm and were irradiated with UV light under gentle stirring using a magnetic stir bar. For UV/H_2O_2 experiments, 10 mg L^{-1} H_2O_2 was added to the samples before UV irradiation. The absorbance of the samples was ≤0.02 cm^{-1} at 254 nm and the light screening (attenuation) coefficient in the Petri dish reactor was calculated to be ≥0.94.[37] The presence of 10 mg L^{-1} of H_2O_2 alone as the control experiment did not induce the gene degradation within 40 min of contact time.[22] The decrease of H_2O_2 by UV photolysis was less than 10% of its initial concentration within the applied UV fluence range (0–300 mJ cm^{-2}). Thus, the degradation of pUC19 by OH radicals (formed from the UV photolysis of H_2O_2) was in a first-order condition throughout the UV irradiation. The reaction solution was sampled (and in UV/H_2O_2 experiments, also supplemented with bovine catalase (40 μg mL^{-1}) to quench residual H_2O_2) and was then stored at −20 °C for 10 days. Triplicate experiments were conducted for each condition, and average sample concentrations (amplicon copies, transforming activity, or viable cell counts) reported with one standard deviation.

Statistical analysis

Statistical analyses were conducted in GraphPad Prism 7 (http://www.graphpad.com/). UV fluence-based first-order rate constants determined from different sets of experiments were compared by multiple linear regression analyses. The null hypothesis in these analyses was that the first-order rate constants were not significantly different, with $p < 0.05$ as the significance cutoff.

Results

Quantitative determination of the transforming activity of plasmid-encoded *amp^R*

Fig. 1 shows that the concentration of transformants after the plasmid transformation increases in proportion to the pUC19 concentration, with a slope of 1.0 in a log–log scale plot. The measured transforming activity ranged from 3.1×10^{-8} to 1.6×10^{-4} for the pUC19 concentrations ranging from 10^{-5} to 5.0×10^{-2} μg mL^{-1}. This result indicates the good capacity of the assay for quantitative determination of the transforming activity. A total of ~2×10^8 transformants were formed per μg of the plasmid. The observed transformation efficiency is comparable to that reported in the literature (*i.e.*, 2×10^8 to 10^9 transformants per μg of plasmid DNA[39]).

The transforming activity of pUC19 (2.5×10^{-2} μg mL^{-1}) after digestion with the *EcoRI* restriction enzyme was found to be ~10^{-6}, which was lower than that of intact pUC19 by a factor of 80. *EcoRI* can linearize pUC19 by DNA cutting.[40] Thus, dsDNA breaks created by *EcoRI*, even outside the *amp^R* gene (especially at restriction site 284, see Fig. S1†), can significantly reduce the ampicillin resistance transforming activity of pUC19. Our data are consistent with other studies showing that the transformation efficiency of plasmids can decrease by two or three orders of magnitude after digestion of the plasmids with various restriction enzymes.[27,41,42] The transforming activities of *amp^R* gene fragments in a range of amplicon sizes (192, 400, 603, and 851 bp, see Fig. S1†) were also determined. These *amp^R* gene fragments (prepared at 10^{11} copies per mL) showed negligible transforming activity (lower by more than four orders of magnitude) as compared to pUC19 at the same molar concentrations. This finding indicates that not only *amp^R* but also the whole plasmid is required for the transformation of *amp^R*.

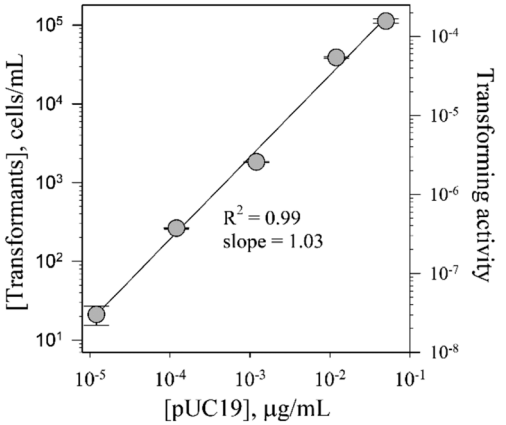

Fig. 1 Concentration of transformants and resulting transforming activity as a function of pUC19 concentration during transformation of *amp^R* to *E. coli* DH5α. The error bars represent one-standard deviation of more than three replicate measurements.

Elimination of transforming activity of plasmid-encoded *amp^R*

Fig. 2 shows decreases in the *amp^R* transforming activity (stars) during UV or UV/H_2O_2 treatment of extracellular (*i.e.*, extracted plasmid) or intracellular (*i.e.*, plasmid within *E. coli*) pUC19 at pH 7. The initial transforming activities in these experiments were ~10^{-4} and the transformation activity of ~10^{-8} was the limit of quantification of the method; thus, a ~4 log reduction could be detected. Without UV and UV/H_2O_2 treatments, *E. coli* and pUC19 were stable for several hours in the phosphate buffer according to the control assays.

The elimination of transforming activity followed first-order kinetics with respect to UV fluence in all cases ($r^2 \geq 0.99$). The fluence-based first-order rate constants (k) for the transforming activity loss could be determined from the slopes of the linear plots (*i.e.*, $k = 2.303 \times$ slope). The k values for intracellular pUC19 (i-ARG) were 6.2(±0.4) × 10^{-2} cm^2 mJ^{-1} for UV treatment (Fig. 2a) and 6.4(±0.4) × 10^{-2} cm^2 mJ^{-1} for

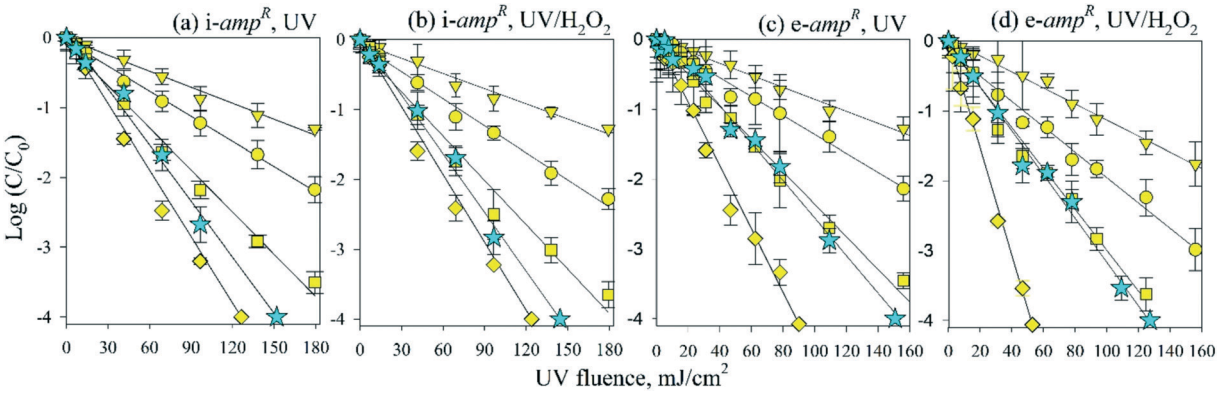

Fig. 2 Logarithmic relative concentration of the transforming activity (★) and amp^R qPCR amplicons (192 bps (▽), 400 bps (○), 603 bps (□) and 851 bps (◇)) as a function of UV fluence during treatment of (a and b) intracellular and (c and d) extracellular pUC19 with (a and c) UV and (b and d) UV/H_2O_2 ($[H_2O_2]_0$ = 10 mg L^{-1}) at pH 7. The symbols represent the measured data and the error bars represent one standard deviation from triplicate experiments. The lines are linear regressions of the data.

UV/H_2O_2 treatment (Fig. 2b), and for extracellular pUC19 (e-ARG) were 6.1(±0.3) × 10^{-2} cm^2 mJ^{-1} for UV (Fig. 2c) and 7.3(±0.4) × 10^{-2} cm^2 mJ^{-1} for UV/H_2O_2 treatment (Fig. 2d), respectively. The data showed that the rates of elimination of the transforming activity were almost the same for all cases, with k of ~6.2 × 10^{-2} cm^2 mJ^{-1} ($p < 0.001$), except for the e-ARG treatment with UV/H_2O_2 yielding a slightly higher (by a factor of 1.2) deactivation rate. At a UV fluence of 40 mJ cm^{-2} (typical for water disinfection), the achieved elimination of the transforming activity was a 1.0 log reduction (1.3 log for UV_{254}/H_2O_2 treatment of e-ARG). To achieve more extensive elimination of the transforming activity such as a 4 log reduction, the required UV fluence was found to be 150 mJ cm^{-2} (125 mJ cm^{-2} for UV_{254}/H_2O_2 treatment of e-ARG).

Degradation of pUC19 fragments (amp^R and *ori* portions) determined by qPCR

Fig. 2 also presents changes in the logarithmic relative concentrations of the suite of variable-length amp^R amplicons measured by qPCR (*i.e.*, 192, 400, 603, and 851 bp) during UV and UV/H_2O_2 treatment of *E. coli* (i-amp^R) and pUC19 plasmid (e-amp^R), respectively. In all cases, the depletion of amp^R genes followed first-order kinetics with respect to the UV fluence ($r^2 \geq 0.99$). The k values determined for the gene damage are summarized in Table 1. The following points from these kinetic data are noteworthy. First, the gene damage rates of amp^R increase with increasing qPCR amplicon size. This result can be explained by the increasing number of target sites for UV (*e.g.*, adjacent pyrimidine dimer sites) with increasing gene size. Second, the gene damage was slower or faster than the transforming activity loss depending on the qPCR amplicon size. For example, the 192 bp gene fragment underwent much slower degradation (by a factor of 2.9–4.0 based on relative k) as compared to the loss of transforming activity. The degradation rates of the 400 and 603 bp gene fragments were higher and closer to the rates of ARG deactivation (*i.e.*, transforming activity elimination). The degradation rates of the 851 bp gene fragment were higher by a factor of 1.1–2.5 as compared to those of the transforming activity loss. These results highlight the need to better understand the relation between the gene damage determined by the qPCR method and the elimination of transforming activity of plasmid-encoded ARGs (further details will be discussed later). Third, the gene damage rates of e-amp^R were higher than those of i-amp^R in both UV and UV/H_2O_2 treatments ($p < 0.05$), and the difference was greater for the UV/H_2O_2 treatment. The gene damage rates of i-amp^R were quite similar between UV and UV/H_2O_2 treatments ($p = 0.47$ for 192 bp, $p = 0.13$ for 400 bp, $p = 0.50$ for 604 bp, and $p = 0.82$ for 851 bp), whereas the gene damage rates of e-amp^R were considerably higher in UV/H_2O_2 than in UV treatment ($p < 0.05$). These results indicated that $^{\bullet}OH$ from UV photolysis of H_2O_2 can contribute to the degradation of extracellular genes, but the effect of $^{\bullet}OH$ on intracellular genes is effectively negligible compared to the UV-induced direct gene damage. A similar result was reported in our previous work, and was explained by complete scavenging of $^{\bullet}OH$ by the cell membrane or cytoplasmic components before reaching i-ARG.[22]

In this study, the qPCR method was also applied to measure the damage in the *ori* region (Fig. S1†), for assessing DNA reactivity outside the amp^R gene in pUC19. Fig. S4† shows decreases in the logarithmic relative concentration of *ori* as measured by the qPCR method with amplicon sizes of 190, 390, and 530 bp during UV and UV/H_2O_2 treatments of extracellular pUC19. The reactivity and degradation patterns of e-*ori* were similar to those of e-amp^R when considering their gene sizes (see the k values in Table 1).

Structural damage to pUC19 measured by gel electrophoresis

Fig. 3a and b present the images of agarose gel electrophoresis analyses of pUC19 (prepared at 5 μg mL^{-1}) before and after UV and UV/H_2O_2 treatments (UV fluence range of 0–312 mJ cm^{-2}). Intact pUC19 yielded a band corresponding to a size slightly larger than the 2 kb molecular weight (MW)

Table 1 Fluence-based rate constants ($k_{CPDs\text{-}I}$ and $k_{CPDs\text{-}II}$) for gene damage quantified by qPCR during treatment of intracellular and extracellular plasmids with UV and UV/H_2O_2

Gene	#base pairs[a]	#TT sites[b]	Plasmid location	k,[c] $cm^2\ mJ^{-1}$	$k_{CPDs\text{-}I}$ (bps),[d] $cm^2\ mJ^{-1}$	$k_{CPDs\text{-}II}$ (TTs),[e] $cm^2\ mJ^{-1}$	Ref.[f]
UV treatment							
amp^R (pUC19)	192	42	Intra	$1.7(\pm0.09) \times 10^{-2}$	3.4×10^{-2}	3.4×10^{-2}	This study
			Extra	$1.9(\pm0.11) \times 10^{-2}$			
	400	67	Intra	$2.8(\pm0.06) \times 10^{-2}$	7.0×10^{-2}	5.5×10^{-2}	
			Extra	$3.1(\pm0.09) \times 10^{-2}$			
	603	96	Intra	$4.6(\pm0.18) \times 10^{-2}$	1.1×10^{-1}	7.9×10^{-2}	
			Extra	$5.4(\pm0.16) \times 10^{-2}$			
	851	118	Intra	$7.2(\pm0.35) \times 10^{-2}$	1.5×10^{-1}	9.7×10^{-2}	
			Extra	$1.0(\pm0.03) \times 10^{-1}$			
ori (pUC19)	190	29	Extra	$1.7(\pm0.09) \times 10^{-2}$	3.3×10^{-2}	2.4×10^{-2}	This study
	390	44	Extra	$2.9(\pm0.12) \times 10^{-2}$	6.9×10^{-2}	3.6×10^{-2}	
	530	59	Extra	$4.0(\pm0.24) \times 10^{-2}$	9.3×10^{-2}	4.8×10^{-2}	
amp^R (pUC4k)	850	119	Intra	6.8×10^{-2}	1.5×10^{-1}	9.8×10^{-2}	Yoon *et al.*, 2017 (ref. 23)
			Extra	1.1×10^{-1}			
kan^R (pUC4k)	806	134	Intra	8.1×10^{-2}	1.4×10^{-1}	1.1×10^{-1}	Yoon *et al.*, 2017 (ref. 23)
			Extra	1.4×10^{-1}			
$bla_{TEM\text{-}1}$	209	30	Extra	5.5×10^{-3}	3.7×10^{-2}	2.5×10^{-2}	Chang *et al.*, 2017 (ref. 28)
	861	123	Extra	6.8×10^{-2}	1.5×10^{-1}	1.0×10^{-1}	
tetA	216	18	Extra	3.8×10^{-2}	3.8×10^{-2}	1.5×10^{-2}	Chang *et al.*, 2017 (ref. 28)
	1200	80	Extra	5.8×10^{-2}	2.1×10^{-1}	6.6×10^{-2}	
UV/H_2O_2 treatment							
amp^R (pUC19)	192	42	Intra	$1.6(\pm0.09) \times 10^{-2}$	3.4×10^{-2}	3.4×10^{-2}	This study
			Extra	$2.5(\pm0.14) \times 10^{-2}$			
	400	67	Intra	$2.9(\pm0.12) \times 10^{-2}$	7.0×10^{-2}	5.5×10^{-2}	
			Extra	$4.1(\pm0.16) \times 10^{-2}$			
	603	96	Intra	$4.8(\pm0.28) \times 10^{-2}$	1.1×10^{-1}	7.9×10^{-2}	
			Extra	$6.7(\pm0.28) \times 10^{-2}$			
	851	118	Intra	$7.3(\pm0.30) \times 10^{-2}$	1.5×10^{-1}	9.7×10^{-2}	
			Extra	$1.8(\pm0.06) \times 10^{-1}$			
ori (pUC19)	190	29	Extra	$2.3(\pm0.05) \times 10^{-2}$	3.3×10^{-2}	2.4×10^{-2}	This study
	390	44	Extra	$3.9(\pm0.14) \times 10^{-2}$	6.9×10^{-2}	3.6×10^{-2}	
	530	59	Extra	$4.7(\pm0.21) \times 10^{-2}$	9.3×10^{-2}	4.8×10^{-2}	
amp^R (pUC4k)	850	119	Intra	6.7×10^{-2}	1.5×10^{-1}	9.8×10^{-2}	Yoon *et al.*, 2017 (ref. 23)
			Extra	1.7×10^{-1}			
kan^R (pUC4k)	806	134	Intra	8.0×10^{-2}	1.4×10^{-1}	1.1×10^{-1}	Yoon *et al.*, 2017 (ref. 23)
			Extra	2.5×10^{-1}			

[a] Total number of base pairs. [b] Total number of TT sites. [c] Fluence-based rate constant measured from this study and the literature. [d] Fluence-based rate constant for CPD formation calculated using $k_{CPDs\text{-}I} = (2.303 \times \varepsilon_{bp} \times \Phi_{CPD})/U$, $\varepsilon_{bp} = \varepsilon_{sbp} \times$ (#base pair) = (15 000 $M^{-1}\ cm^{-1}$) × (#base pair), and $\Phi_{CPD} = 2.4 \times 10^{-3}$ (Görner, 1994).[26] [e] Calculated using $k_{CPDs\text{-}II} = (2.303 \times \varepsilon_{TT} \times \Phi_{TT})/U$, $\varepsilon_{TT} = \varepsilon_{sTT,254} \times$ (#TT) = (8400 $M^{-1}\ cm^{-1}$) × (#TT), and $\Phi_{TT} = 2.0 \times 10^{-2}$ (Douki *et al.*, 2000).[50] [f] Source for the measured k values.

marker, and pUC19 treated within *EcoRI* showed a band corresponding to a size slightly larger than the 3 kb MW marker. The observed band positions are consistent with the size of pUC19 (*i.e.*, 2686 bp) and the fact that plasmids typically exist in a supercoiled form (*i.e.*, intact pUC19), which migrates faster than the linear form (*i.e.*, *EcoRI*-treated pUC19) in an agarose gel because of their conformational difference. After the UV treatment, the band position of pUC19 changed negligibly. In contrast, the band gradually moved upward with increasing UV fluence during UV/H_2O_2 treatment, indicating the conformational change of pUC19 from the supercoiled to linear form. On the basis of quantitative agarose gel image analyses,[36] the degree of linearization of pUC19 was found to be less than 10% during the UV treatment but increased up to 93% during the UV/H_2O_2 treatment with an increase in UV fluence up to 312 mJ cm^{-2} (Fig. S5†). These results can be explained by the fact that UV mainly induces damage to the DNA bases such as CPDs[26,27] that is not detected in the agarose gel analysis. During UV/H_2O_2 treatment, $^{\bullet}OH$ is formed and reacts with not only DNA bases but also the sugar phosphate

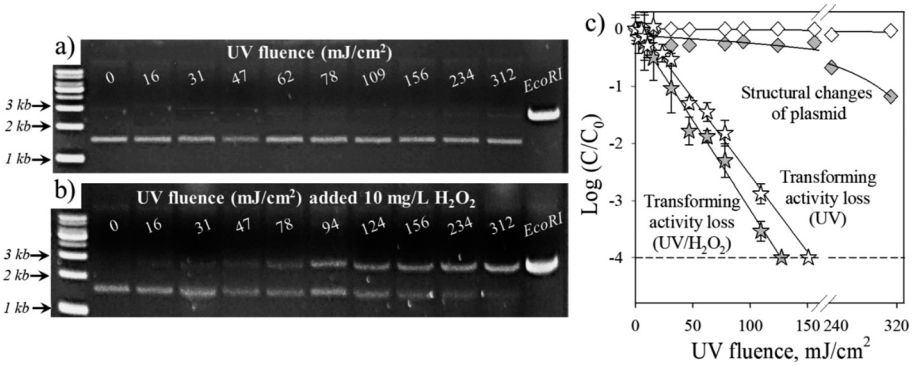

Fig. 3 Agarose gel electrophoresis images of extracellular pUC19 plasmids treated with (a) UV and (b) UV/H_2O_2 ($[H_2O_2]_0$ = 10 mg L^{-1}) as a function of UV fluence (0–312 mJ cm^{-2}). The first column shows gel images of standard ladders. The last column shows gel images of the pUC19 plasmid treated by the restriction enzyme (*EcoRI*). (c) Logarithmic-scale decreases of the structural integrity (from quantitative analysis of the electrophoresis images) and transforming activity of pUC19 as a function of UV fluence.

backbone; the latter reaction can cause significant DNA damage such as dsDNA breaks[30] that are detectable by agarose gel analysis. Finally, the rates of the plasmid structural (conformational) change were compared to the rates of transforming activity loss during UV and UV/H_2O_2 treatments. Fig. 3c shows that the transforming activity loss occurred much faster than the structural degradation of the plasmid during UV and UV/H_2O_2 treatments. This finding indicates that the UV-induced damage to DNA bases is mainly responsible for the elimination of the transforming activity of plasmid-encoded ARGs. A similar conclusion has been reached in other studies.[22,28]

Discussion

Effects of DNA repair and plasmid characteristics on the efficiency of elimination of transforming activity

The efficiency of elimination of pUC19's transforming activity during UV irradiation, determined in this study, can be compared with that in other studies, in which several different plasmids were treated with UV (254 nm) and transformed into several strains of *E. coli* mutants[43] or *Acinetobacter baylyi*[28] as host cells. Table 2 summarizes the *k* values for the elimination of transforming activity and corresponding information on the plasmids and host cells used in these studies. Note that these plasmids (pUC19, pTZ18R, pBR322, and pWH1266) all contain a β-lactamase resistance gene (either amp^R or bla_{TEM-1}). pBR322 and pWH1266 also contain a tetracycline resistance gene (*tetA*).

Data from previous work reveals that the efficiency of elimination of transforming activity is greatly influenced by the type of *E. coli* recipient strain. When *E. coli* AB2480 (a double-mutant strain lacking both *uvrA* and *recA* genes) was used as a recipient strain, the *k* value for UV-induced elimination of transforming activity was 5.3×10^{-1} cm^2 mJ^{-1} for pTZ18R and 6.7×10^{-1} cm^2 mJ^{-1} for pBR322. These values are 22- and 15-fold larger than the *k* value for pTZ18R (2.4×10^{-2} cm^2 mJ^{-1}) and pBR322 (4.4×10^{-2} cm^2 mJ^{-1}) when *E. coli* AB1157 (wild-type strain) was used. Relatively low-to-intermediate levels of *k*

Table 2 Fluence-based rate constants (k_{CPDs-I} and $k_{CPDs-II}$) for the elimination of transforming activity of ARGs during UV treatment of extracellular plasmids

Plasmid	#base pairs[a]	#TT sites[b]	Host cell for transformation	*k*,[c] cm^2 mJ^{-1}	k_{CPDs-I} (bps),[d] cm^2 mJ^{-1}	$k_{CPDs-II}$ (TTs),[e] cm^2 mJ^{-1}	Ref.[f]
pUC19	2686	383	*E. coli* DH5α (recA$^-$)	6.1×10^{-2}	4.7×10^{-1}	3.1×10^{-1}	This study
pTZ18R	2861	453	*E. coli* K12 AB2480 (uvrA$^-$, recA$^-$)	5.3×10^{-1}	5.0×10^{-1}	3.7×10^{-1}	Gurzadyan *et al.*, 1993 (ref. 43)
			E. coli K12 AB1886 (uvrA$^-$)	7.1×10^{-2}			
			E. coli K12 AB2463 (recA$^-$)	6.7×10^{-2}			
			E. coli K12 AB1157 (wild type)	2.4×10^{-2}			
pBR322	4361	513	*E. coli* K12 AB2480 (uvrA$^-$, recA$^-$)	6.7×10^{-1}	7.7×10^{-1}	4.2×10^{-1}	Gurzadyan *et al.*, 1993 (ref. 43)
			E. coli K12 AB1157 (wild type)	4.4×10^{-2}			
pWH1266	8890	—[g]	*Acinetobacter baylyi*	1.1×10^{-1}	1.56	—[g]	Chang *et al.*, 2017 (ref. 28)

[a] Total number of base pairs. [b] Total number of TT sites. [c] Fluence-based rate constant measured from this study and the literature. [d] Fluence-based rate constant for CPD formation calculated using $k_{CPDs-I} = (2.303 \times \varepsilon_{bp} \times \Phi_{CPD})/U$, $\varepsilon_{bp} = \varepsilon_{sbp} \times$ (#base pair) = (15 000 M^{-1} cm^{-1}) × (#base pair), and $\Phi_{CPD} = 2.4 \times 10^{-3}$ (Görner, 1994).[26] [e] Calculated using $k_{CPDs-II} = (2.303 \times \varepsilon_{TT} \times \Phi_{TT})/U$, $\varepsilon_{TT} = \varepsilon_{sTT,254} \times$ (#TT) = (8400 M^{-1} cm^{-1}) × (#TT), and $\Phi_{TT} = 2.0 \times 10^{-2}$ (Douki *et al.*, 2000).[50] [f] Source for the measured *k* values. [g] Not available because the full gene sequence is not known.

were observed for pTZ18R when single-mutant *E. coli* AB1886 (deficient in *uvrA*, $k = 7.1 \times 10^{-2}$ cm^2 mJ^{-1}) and *E. coli* AB2463 (deficient in *recA*, $k = 6.7 \times 10^{-2}$ cm^2 mJ^{-1}) strains were tested.[43] These results can be explained by the different levels of DNA repair ability of the host cells. *uvrA* is one of the *uvr* genes responsible for DNA repair through the nucleotide excision repair (NER) pathway.[44] The *recA* gene is involved in various types of homologous recombination and is essential for the repair and maintenance of DNA in prokaryotes.[45] Thus, the DNA repair in double-mutant *E. coli* AB2480 was negligible and resulted in a highly efficient loss of plasmid transforming activity. In contrast, DNA repair was significant in the other *E. coli* strains (*i.e.*, single-mutant and wild-type strains), resulting in much slower elimination of the transforming activity.

The k value determined here for UV-induced deactivation of pUC19 in *E. coli* DH5α (=6.1×10^{-2} cm^2 mJ^{-1}) is close to that for pTZ18R in the *E. coli* AB2463 strain (=6.7×10^{-2} cm^2 mJ^{-1}). Of note, both *E. coli* strains are deficient in the *recA* gene, and the sizes of the two plasmids are comparable (2686 bp for pUC19 and 2861 bp for pTZ18R, Table 2). The k value for pWH1266 and wild-type *A. baylyi* is 1.1×10^{-1} cm^2 mJ^{-1},[28] which is larger than that for pTZ18R and pBR322 with wild-type *E. coli* by a factor of 4.6 and 2.5, respectively. Notably, the size of pWH1266 is larger than that of pTZ18R and pBR322 by a factor of 3.1 and 2.0, respectively. Larger plasmids will typically contain a greater number of potential DNA damage sites and would accordingly be expected to show a higher rate of UV-induced elimination of transforming activity.

The rate of pyrimidine dimer formation *vs.* elimination of transforming activity of the plasmid

CPDs and 6-4 photoproducts are known as the major types of UV-induced DNA damage.[26,27,46] These types of DNA damage are readily formed at adjacent pyrimidine sites such as intrastrand thymine–thymine (TT), thymine–cytosine (TC), cytosine–thymine (CT), and cytosine–cytosine (CC) doublets. The formation of CPDs usually predominates over the formation of 6-4 photoproducts. In addition, the TT site is the most photoreactive in terms of CPD formation among the bipyrimidine doublets.[47,48] For instance, the following average quantum yields of CPD formation (in the number of CPDs formed per number of photons absorbed by the entire target DNA) have been reported during UV_{254} irradiation of dsDNA under solutions conditions ranging from pure water-0.2 M ionic strength; $0.66 \times 10^{-3} : 0.23 \times 10^{-3} : 0.10 \times 10^{-3} : 0.02 \times 10^{-3}$ for TT : TC : CT : CC.[48] The TC site also shows a high yield for the 6-4 photoproduct with a quantum yield of 0.19×10^{-3}.[48] In light of this, we attempted to analyze the relationship between the formation rate of CPDs as the major UV-induced DNA damage and consequent elimination of the transforming activity of plasmid pUC19.

The UV fluence-based formation rate constant of CPDs (k_{CPDs}, cm^2 mJ^{-1}) in dsDNA can be written as eqn (2):

$$k_{CPDs} = (2.303 \times \varepsilon \times \Phi_{CPDs}) \div U \quad (2)$$

where ε (M^{-1} cm^{-1}) is the molar absorption coefficient, Φ_{CPDs} (mol per Einstein) is the quantum efficiency of CPD formation, and U (= 4.72×10^5 J per Einstein) is the molar photon energy at 254 nm [ref. 38 and references therein]. The Φ_{CPDs} values reported for dsDNA show variations due to different ways of defining the quantum yield. A Φ_{CPDs} value of ~2.4×10^{-3} (Görner, 1994 (ref. 26)) or ~1.0×10^{-3} (ref. 48) was obtained by considering the number of CPDs formed per photon absorbed by the entire target DNA.[48] In this case (approach I, $k_{CPDs\text{-}I}$), the ε value for the entire target DNA should be used. The ε value for all base pairs in a strand of dsDNA can be conveniently estimated as $\varepsilon_{bp} = \varepsilon_{sbp} \times$ (# of base pairs) in which ε_{sbp} is the average molar absorption coefficient of a single base pair (ε_{sbp} = 15 000 M^{-1} cm^{-1} (ref. 49)), and "# of base pairs" is the total number of base pairs in a given DNA. Alternatively, the quantum yield could be defined based on the photons absorbed specifically by two adjacent pyrimidines. In the current study, we focused on photon absorbance by TT sites, as they are the most photoreactive for CPD formation amongst the four pyrimidine doublets TT, TC, CT, and CC, and also reported to be the most slowly repaired in human skin cells.[46] In the case of TT sites (approach II, $k_{CPDs\text{-}II}$), a Φ_{TT} value of ~2.0×10^{-2} has been reported.[47,51] The ε value for all TT sites within a strand of dsDNA can be calculated as $\varepsilon_{TT} = \varepsilon_{sTT,254} \times$ (#TT), where ε_{sTT} is the molar absorption coefficient of a single TT site (=8400 M^{-1} cm^{-1} (ref. 51)) and #TT is the number of TT sites in a given DNA. Using the two different definitions of Φ_{CPDs} described above, $k_{CPDs\text{-}I}$ and $k_{CPDs\text{-}II}$ can be calculated for plasmids as a function of the number of base pairs and TT sites, respectively.

Fig. 4 and S6† show a comparison of the calculated k_{CPDs} values (dashed lines) with the measured k values for the elimination of transforming activity (symbols) from this study (pUC19) and from the literature (pTZ18R, pBR322, and pWH1266) as a function of the number of (a) base pairs ($k_{CPDs\text{-}I}$) and (b) TT sites ($k_{CPDs\text{-}II}$) in the plasmids. In addition, a Φ_{TT} value of 2.0×10^{-2} was used for Fig. 4b and S6b.† Notably, k_{CPDs} ($k_{CPDs\text{-}I}$ and $k_{CPDs\text{-}II}$) were close to k measured when double-mutant *E. coli* was used as a recipient (differences ranging from factors of 1 to 2.3). This finding indicates that in the double-mutant strain, most of the CPDs formed in the plasmids led to the elimination of transforming activity because the CPDs were not repaired in the corresponding host cell. The k values obtained with single mutants and wild-type *E. coli* and *A. baylyi* strains were significantly lower than k_{CPDs} by factors ranging from 5 to 15 (indicated as the ratio of the slopes compared to k_{CPDs}, Fig. 4). This result strongly suggests the significant role of CPD repair activity in these host cells. One alternative explanation for these trends may be that some DNA damages on the plasmid are located where they do not inhibit the plasmid transformation, which requires further investigation. Overall, good linear trends were found between the measured k values and the number of base pairs and TT sites in the plasmids. These trends can be explained by the fact that more CPDs are formed with increasing gene fragment size, or – more specifically –

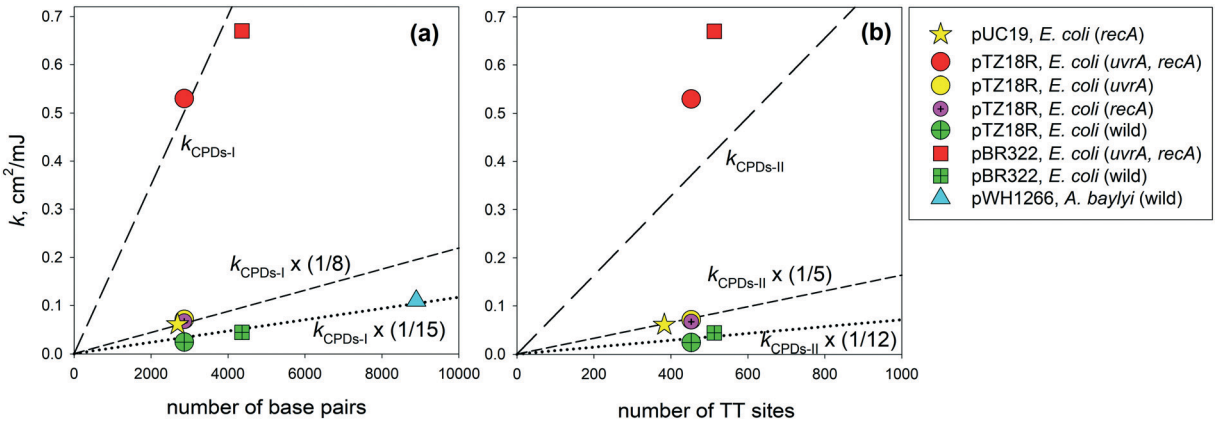

Fig. 4 UV fluence-based rate constants (k) for elimination of transforming activity of plasmids as a function of the number of (a) base pairs (k_{CPDs-I}) and (b) TT sites ($k_{CPDs-II}$). The k data were obtained from this study (pUC19) and taken from Gurzadyan *et al.*, 1993 (pTZ18r and pBR322)[43] and Chang *et al.*, 2017 (pWH1266)[28] (see Table 2). The long-dash lines indicate the rate constants calculated for CPD formation across the entire plasmid (k_{CPDs}). For (a), a Φ_{CPD} value[26] of 2.4×10^{-3} was used to calculate the k_{CPDs-I} for the photons absorbed by the entire DNA. For (b), a Φ_{TT} value[50] of 2.0×10^{-2} was used to calculate the $k_{CPDs-II}$ for the photons absorbed by all TT sites within the entire DNA. The short-dash and dotted lines are the k_{CPDs} multiplied with slope factors (ranging from 1/15 to 1/5) that were obtained to fit the measured k values. See the main text for further explanation.

increasing number of potential pyrimidine dimer sites. The observed linear relation can be further tested in future studies by determining k for plasmids with different gene fragment sizes and compositions, and in host cells with different DNA repair abilities.

The rate of pyrimidine dimer formation *vs.* gene damage measured by qPCR

Fig. 5 and S7† depict the plots of the measured k values (symbols) for the degradation of target qPCR amplicons as a function of (a) the number of base pairs and (b) the number of TT sites in the genes. In addition, k values were compared with the k_{CPDs-I} and $k_{CPDs-II}$ values of the target genes that could be calculated *via* eqn (2) and the method described above (Φ_{CPD} of 2.4×10^{-3} for Fig. 5a, 1.0×10^{-3} for Fig. S7a,† and Φ_{TT} of 2.0×10^{-2} for Fig. 5b and S7b†). The k data from the UV treatment of extracellular and intracellular plasmids as well as the k data from the UV/H_2O_2 treatment of intracellular plasmids (but not extracellular plasmids) from this study and from the literature were included in the plots (Table 1). The UV/H_2O_2 data for i-ARGs were included because the damage to intracellular genes during UV/H_2O_2 treatment was exclusively caused by UV, with little contribution from $^{\bullet}$OH. The k values for extracellular plasmids during UV/H_2O_2 treatment were not included because they were much larger compared to those of UV treatment, indicating a significant contribution of $^{\bullet}$OH reactions to extracellular gene damage.

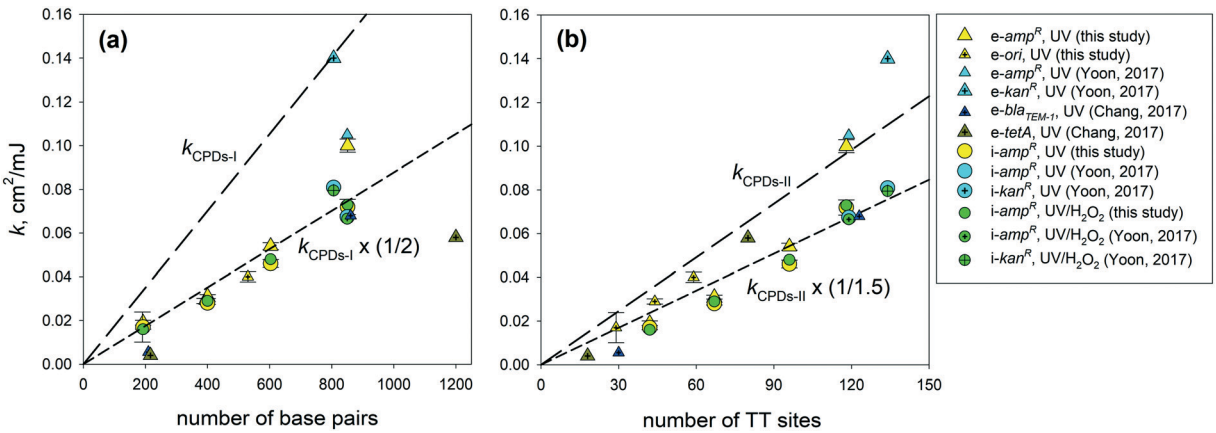

Fig. 5 UV fluence-based rate constants (k) for gene damage of extracellular (e-ARGs, triangles) and intracellular (i-ARGs, circles) plasmid-encoded genes as a function of the number of (a) base pairs (k_{CPD-I}) and (b) TT sites (k_{CPD-II}). The k data were obtained from this study, and taken from Yoon *et al.*,[22] 2017 and Chang *et al.*,[28] 2017 (see Table 1). The long-dash lines indicate the calculated rate constant for the CPD formation (k_{CPDs}). For (a), a Φ_{CPD} value[26] of 2.4×10^{-3} was used to calculate, and for (b), a Φ_{TT} value[50] of 2.0×10^{-2} was used to calculate. The short-dash lines are linear regressions of the k values of intracellular genes in which the relative slope of k compared to k_{CPDs} is indicated. See Fig. 4 and the main text for further explanation.

The following points are noteworthy and arise from the results in Fig. 5. First, the intracellular genes (circles) show good linear relations with the numbers of base pairs and TT sites (dashed lines, $r^2 = 0.93$ for both cases), whereas k values for the extracellular genes (triangles) correlated relatively poorly with the numbers of base pairs and TT sites. Second, the number of TT sites ($k = (6.4 \times 10^{-4}) \times$ (# of TT sites), $r^2 = 0.77$, $n = 25$) yielded a better linear correlation with k as compared to the number of base pairs ($k = (8.9 \times 10^{-5}) \times$ (# of base pairs), $r^2 = 0.65$, $n = 25$) when both extracellular and intracellular genes were considered. This result can again be explained by the fact that UV-induced lesions accumulate most rapidly at TT sites. Consistent with this notion, k values reported for *tetA* (216 and 1200 bp)[28] were much lower than the other k values shown in Fig. 5a because the *tetA* gene contains fewer TT sites for the same total number of base pairs (Table 1). Third, k values for the gene damage were close to k_{CPDs}. When compared on the basis of the total base pairs, the predicted $k_{CPDs\text{-}I}$ values exceeded the measured k values by a factor of ~2 when a Φ_{CPD} of 2.4×10^{-3} (ref. 26) was used (Fig. 5a) but were similar to the measured k values when a Φ_{CPD} of 1.0×10^{-3} (ref. 48) was used (Fig. S7a†). The variation in the CPD quantum yields in the literature could be attributed to different analytical methods for quantifying the dimeric photoproducts (*e.g.*, acid hydrolysis, chromatographic separation, and quantification by radioactivity or mass spectrometry) or experimental conditions (*e.g.*, DNA concentration, ionic strength). When compared on the basis of total TT sites, the predicted $k_{CPDs\text{-}II}$ values exceeded the measured k values by a factor of 1.5 (Fig. 5b). This level of difference in k (*i.e.*, within a factor of 2) can be considered minor, given the assumptions and uncertainties of the parameters in the k_{CPDs} calculation. Thus, further attempts to improve the kinetic model for $k_{CPDs\text{-}II}$ prediction by considering the photoproducts of bipyrimidine doublets other than TT were not pursued.

Overall, our results indicate that the qPCR method is sensitive enough to detect most major UV-induced DNA damages (*e.g.*, CPDs). This finding is consistent with other studies, which show that the PCR amplification efficiency of genes containing a CPD is drastically reduced (by $\sim 2 \log_{10}$) compared to the intact gene.[52]

Enhanced degradation of extracellular ARGs and its impact on elimination of the transforming activity

The kinetic data on gene damage from this study and from the literature suggest that extracellular genes sometimes undergo more rapid degradation (by a factor of up to 1.7) than the corresponding intracellular genes during UV irradiation.[22] This phenomenon was particularly noticeable for some long amplicons (*i.e.*, amp^R and kan^R: 806–851 bp long). The higher reactivity of extracellular genes may have been caused by incidental photochemical reactions of metal–DNA complexes. In particular, photolysis of Cu(II)–DNA complexes has been known to produce Cu(I) and reactive oxygen species (ROS) including $^{\bullet}OH$, which can initiate oxidative DNA damage.[53] Even though the plasmid samples in this study were isolated from *E. coli* with a purification step (*i.e.*, washing with phosphate buffer), a certain amount of Cu(II) complexed with DNA could have remained. This explanation can be supported by the observation that the degradation rate of e-amp^R amplicons during UV irradiation of pUC19 decreased by a factor of 1.1–1.7 ($p < 0.05$) after the addition of EDTA (0.1 mM) or methanol (10 mM; Fig. S8†). EDTA can lower the photoreactivity of Cu(II)–DNA complexes by forming a less photoreactive metal–EDTA complex.[54] Methanol can protect DNA by scavenging $^{\bullet}OH$.[30] Furthermore, the degradation rate of e-amp^R increased by a factor of ~1.3 ($p < 0.05$) after the addition of $CuSO_4$ (10 μM; Fig. S8†). Similar photochemical reactions of Cu(II)–DNA complexes could have proceeded and contributed to the enhanced degradation of the extracellular genes. Nonetheless, this was not the case for the intracellular genes, presumably owing to significant scavenging of UV-induced ROS by intracellular reductants (*e.g.*, sulfur-containing proteins). In agreement with these data, the degradation of extracellular ARGs was significantly enhanced by H_2O_2 addition during UV irradiation of plasmids (Fig. 2 and Table 1), whereas no impact of H_2O_2 addition was observed for intracellular ARGs, owing to nearly complete scavenging of $^{\bullet}OH$ by intracellular components.[22] These observations may in turn provide an explanation for the relatively poor correlations of measured k values with the number of base pairs or TT sites for extracellular ARGs in comparison with intracellular ARGs (Fig. 5).

It is noteworthy that the enhanced degradation of extracellular ARGs beyond the direct UV-induced damage does not lead to more rapid elimination of the transforming activity. The rate of elimination of transforming activity was nearly constant across the UV and UV/H_2O_2 treatments of e-ARGs, while the gene degradation rates varied by a factor of up to 1.8 ($p < 0.05$) for the same treatments (Fig. 2 and Table 1). Thus, the damage to extracellular ARGs by UV, $^{\bullet}OH$, or other ROS was detectable by the qPCR method, but in the *E. coli* transformation assay, only the direct UV-induced gene damage could be detected. This finding could be due to efficient repair of the gene damage caused by $^{\bullet}OH$ (or other ROS) in the *E. coli* transformation system. Single oxidized bases (*e.g.*, 5,6-dihydroxy-5,6-dihydrothymine) are the most frequent type of nucleobase damage in cellular DNA from exposure to $^{\bullet}OH$, and most of such lesions are efficiently removed by the cellular base excision repair system.[55] Such DNA repair function does not exist in the qPCR system. In addition to the DNA repair, the difference in fidelity between *E. coli* DNA polymerase and *Taq* DNA polymerase could have played a role. *E. coli* is known to possess specialized lesion bypass DNA polymerases with low fidelity that enable translesion replication of damaged DNA.[56,57] In contrast, the *Taq* polymerase of the qPCR method is a relatively high-fidelity polymerase with high enough sensitivity to detect even minor single-base lesions.[52]

Conclusions

- Under typical UV fluences for disinfection purposes (*e.g.*, 40 mJ cm^{-2}), a ~1 log reduction in the transforming activity

of a plasmid-encoded ARG is expected. To achieve more extensive elimination of the transforming activity (*e.g.*, >4 log reduction), a UV fluence of more than 150 mJ cm^{-2} is required. Addition of H_2O_2 (*i.e.*, the UV/H_2O_2 advanced oxidation process) does not significantly enhance the efficiency of elimination of the transforming activity.

• The efficiency of elimination of the transforming activity for a plasmid-encoded ARG during UV treatment depends on the rate of formation of CPDs in the plasmid and the repair of such DNA damage during the transformation process in host cells. Significant capacity for CPD repair is present in the *E. coli* recipient strain (DH5α) used in this study and is also expected in many wild-type bacterial cells.

• The rate of formation of CPDs can be calculated by considering the number of TT sites in the target gene fragments or whole plasmids and the TT-specific photochemical reaction parameters (*i.e.*, $\Phi_{TT} = 2.0 \times 10^{-2}$ and $\varepsilon_{TT} = 8400\ M^{-1}\ cm^{-1}$ for 254 nm light). Additionally, CPDs can be sensitively detected and quantified by qPCR.

• CPD formation is the major DNA damage mechanism and responsible for the elimination of transforming activity of extra- and intracellular plasmids during UV and UV/H_2O_2 treatments.

• For extracellular plasmids, DNA base oxidation takes place in addition to CPD formation, and these lesions are detectable by the qPCR method. The DNA base oxidation, however, does not reduce the transforming activity of pUC19 in the *E. coli* recipient strain (DH5α) utilized here.

Conflicts of interest

There are no conflicts to declare.

Acknowledgements

This study was supported by the National Research Foundation funded by the Ministry of Science, ICT & Future Planning (NRF-2017R1A2B2002593) and the Korea Environmental Industry & Technology Institute (KEITI-2015001800001). Additional support for MCD from the U.S. National Science Foundation Award CBET-1254929 is gratefully acknowledged.

References

1 World Health Organization, *Antimicrobial resistance: global report on surveillance*, WHO, 2014.
2 H. K. Allen, J. Donato, H. H. Wang, K. A. Cloud-Hansen, J. Davies and J. Handelsman, Call of the wild: Antibiotic resistance genes in natural environments, *Nat. Rev. Microbiol.*, 2010, **8**(4), 251.
3 T. U. Berendonk, C. M. Manaia, C. Merlin, D. Fatta-Kassinos, E. Cytryn and F. Walsh, *et al.*, Tackling antibiotic resistance: The environmental framework, *Nat. Rev. Microbiol.*, 2015, **13**(5), 310.
4 A. Pruden, Balancing water sustainability and public health goals in the face of growing concerns about antibiotic resistance, *Environ. Sci. Technol.*, 2014, **48**(1), 5–14.
5 C. M. Thomas and K. M. Nielsen, Mechanisms of, and barriers to, horizontal gene transfer between bacteria, *Nat. Rev. Microbiol.*, 2005, **3**, 711.
6 P. J. Vikesland, A. Pruden, P. J. J. Alvarez, D. Aga, H. Bürgmann and X.-D. Li, *et al.*, Toward a comprehensive strategy to mitigate dissemination of environmental sources of antibiotic resistance, *Environ. Sci. Technol.*, 2017, **51**(22), 13061–13069.
7 L. Rizzo, C. Manaia, C. Merlin, T. Schwartz, C. Dagot and M. C. Ploy, *et al.*, Urban wastewater treatment plants as hotspots for antibiotic resistant bacteria and genes spread into the environment: A review, *Sci. Total Environ.*, 2013, **447**, 345–360.
8 D. T. Tan and D. Shuai, Research highlights: Antibiotic resistance genes: From wastewater into the environment, *Environ. Sci.: Water Res. Technol.*, 2015, **1**(3), 264–267.
9 H. Chen and M. Zhang, Effects of advanced treatment systems on the removal of antibiotic resistance genes in wastewater treatment plants from Hangzhou, China, *Environ. Sci. Technol.*, 2013, **47**(15), 8157–8163.
10 N. Czekalski, T. Berthold, S. Caucci, A. Egli and H. Bürgmann, Increased levels of multiresistant bacteria and resistance genes after wastewater treatment and their dissemination into Lake Geneva, Switzerland, *Front. Microbiol.*, 2012, **3**, 106.
11 J. G. Jacangelo and R. R. Trussell, International report: Water and wastewater disinfection-trends, issues and practices, *Water Sci. Technol.: Water Supply*, 2002, **2**(3), 147–157.
12 Y. Lee and U. Von Gunten, Advances in predicting organic contaminant abatement during ozonation of municipal wastewater effluent: Reaction kinetics, transformation products, and changes of biological effects, *Environ. Sci.: Water Res. Technol.*, 2016, **2**(3), 421–442.
13 D. Gerrity, Y. Lee, S. Gamage, M. Lee, A. N. Pisarenko and R. A. Trenholm, *et al.*, Emerging investigators series: Prediction of trace organic contaminant abatement with UV/H_2O_2: Development and validation of semi-empirical models for municipal wastewater effluents, *Environ. Sci.: Water Res. Technol.*, 2016, **2**(3), 460–473.
14 D. B. Miklos, R. Hartl, P. Michel, K. G. Linden, J. E. Drewes and U. Hübner, UV/H_2O_2 process stability and pilot-scale validation for trace organic chemical removal from wastewater treatment plant effluents, *Water Res.*, 2018, **136**, 169–179.
15 J. Alexander, G. Knopp, A. Dötsch, A. Wieland and T. Schwartz, Ozone treatment of conditioned wastewater selects antibiotic resistance genes, opportunistic bacteria, and induce strong population shifts, *Sci. Total Environ.*, 2016, **559**, 103–112.
16 M. C. Dodd, Potential impacts of disinfection processes on elimination and deactivation of antibiotic resistance genes during water and wastewater treatment, *J. Environ. Monit.*, 2012, **14**(7), 1754–1771.
17 G. Ferro, F. Guarino and A. Cicatelli, Rizzo L. β-lactams resistance gene quantification in an antibiotic resistant *Escherichia coli* water suspension treated by advanced

oxidation with UV/H_2O_2, *J. Hazard. Mater.*, 2017, **323**, 426–433.

18 F. Lüddeke, S. Heß, C. Gallert, J. Winter, H. Güde and H. Löffler, Removal of total and antibiotic resistant bacteria in advanced wastewater treatment by ozonation in combination with different filtering techniques, *Water Res.*, 2015, **69**, 243–251.

19 C. W. McKinney and A. Pruden, Ultraviolet disinfection of antibiotic resistant bacteria and their antibiotic resistance genes in water and wastewater, *Environ. Sci. Technol.*, 2012, **46**(24), 13393–13400.

20 G. Pak, D. E. Salcedo, H. Lee, J. Oh, S. K. Maeng and K. G. Song, *et al.*, Comparison of antibiotic resistance removal efficiencies using ozone disinfection under different pH and suspended solids and humic substance concentrations, *Environ. Sci. Technol.*, 2016, **50**(14), 7590–7600.

21 J. M. Sousa, G. Macedo, M. Pedrosa, C. Becerra-Castro, S. Castro-Silva and M. F. R. Pereira, *et al.*, Ozonation and UV254nm radiation for the removal of microorganisms and antibiotic resistance genes from urban wastewater, *J. Hazard. Mater.*, 2017, **323**, 434–441.

22 Y. Yoon, H. J. Chung, D. Y. Wen Di, M. C. Dodd, H.-G. Hur and Y. Lee, Inactivation efficiency of plasmid-encoded antibiotic resistance genes during water treatment with chlorine, UV, and UV/H_2O_2, *Water Res.*, 2017, **123**, 783–793.

23 N. Czekalski, S. Imminger, E. Salhi, M. Veljkovic, K. Kleffel and D. Drissner, *et al.*, Inactivation of antibiotic resistant bacteria and resistance genes by ozone: from laboratory experiments to full-scale wastewater treatment, *Environ. Sci. Technol.*, 2016, **50**(21), 11862–11871.

24 M. Colomer-Lluch, J. Jofre and M. Muniesa, Antibiotic Resistance Genes in the Bacteriophage DNA Fraction of Environmental Samples, *PLoS One*, 2011, **6**(3), e17549.

25 Y. Zhang, A. Li, T. Dai, F. Li, H. Xie and L. Chen, *et al.*, Cell-free DNA: A neglected source for antibiotic resistance genes spreading from WWTPs, *Environ. Sci. Technol.*, 2018, **52**(1), 248–257.

26 H. Görner, New trends in photobiology: Photochemistry of DNA and related biomolecules: Quantum yields and consequences of photoionization, *J. Photochem. Photobiol., B*, 1994, **26**(2), 117–139.

27 R. P. Sinha and D.-P. Hader, UV-induced DNA damage and repair: A review, *Photochem. Photobiol. Sci.*, 2002, **1**(4), 225–236.

28 P. H. Chang, B. Juhrend, T. M. Olson, C. F. Marrs and K. R. Wigginton, Degradation of extracellular antibiotic resistance genes with UV254 treatment, *Environ. Sci. Technol.*, 2017, **51**(11), 6185–6192.

29 R. Destiani, M. R. Templeton and W. Kowalski, Relative ultraviolet sensitivity of selected antibiotic resistance genes in waterborne bacteria, *Environ. Eng. Sci.*, 2017, DOI: 10.1089/ees.2017.0179.

30 C. Von Sonntag, *Free-radical-induced DNA damage and its repair: A chemical perspective*, Springer Science & Business Media, 2006.

31 E. Luby, A. M. Ibekwe, J. Zilles and A. Pruden, Molecular methods for assessment of antibiotic resistance in agricultural ecosystems: Prospects and challenges, *J. Environ. Qual.*, 2016, **45**(2), 441–453.

32 N. Casali and A. Preston, *E. coli plasmid vectors: Methods and applications*, Springer Science & Business Media, 2003.

33 Bioneer, *AccuPrep*® Nano-Plus Plasmid Mini/Midi/Maxi Extraction Kit, User's Guide, Korea, Available at http://us.bioneer.com/Protocol/AccuPrep%20Nano-Plus%20Plasmid%20Extraction%20Kit.pdf, 2016.

34 D. Hanahan, Studies on transformation of *Escherichia coli* with plasmids, *J. Mol. Biol.*, 1983, **166**(4), 557–580.

35 D. Shanehbandi, A. A. Saei, H. Zarredar and A. Barzegari, Vibration and glycerol-mediated plasmid DNA transformation for *Escherichia coli*, *FEMS Microbiol. Lett.*, 2013, **348**(1), 74–78.

36 C. A. Schneider, W. S. Rasband and K. W. Eliceiri, NIH Image to ImageJ: 25 years of image analysis, *Nat. Methods*, 2012, **9**, 671.

37 J. R. Bolton and K. G. Linden, Standardization of methods for fluence (UV dose) determination in bench-scale UV experiments, *J. Environ. Eng.*, 2003, **129**(3), 209–215.

38 Y. Lee, D. Gerrity, M. Lee, S. Gamage, A. Pisarenko and R. A. Trenholm, *et al.*, Organic contaminant abatement in reclaimed water by UV/H_2O_2 and a combined process consisting of O_3/H_2O_2 followed by UV/H_2O_2: prediction of abatement efficiency, energy consumption, and byproduct formation, *Environ. Sci. Technol.*, 2016, **50**(7), 3809–3819.

39 D. Hanahan, J. Jessee and F. R. Bloom, Plasmid transformation of *Escherichia coli* and other bacteria, *Methods Enzymol.*, 1991, 63–113.

40 A. Pingoud and A. Jeltsch, Structure and function of type II restriction endonucleases, *Nucleic Acids Res.*, 2001, **29**(18), 3705–3727.

41 R. Palmen, B. Vosman, P. Buijsman, C. K. D. Breek and K. J. Hellingwerf, Physiological characterization of natural transformation in *Acinetobacter calcoaceticus*, *Microbiology*, 1993, **139**(2), 295–305.

42 D. Schulte-Frohlinde, Biological consequences of strand breaks in plasmid and viral DNA, *Br. J. Cancer, Suppl.*, 1987, **8**, 129–134.

43 G. G. Gurzadyan, H. Gorner and D. Schulte-Frohlinde, Photolesions and biological inactivation of plasmid DNA on 254nm irradiation and comparison with 193nm laser irradiation, *Photochem. Photobiol.*, 1993, **58**(4), 477–485.

44 C. Kisker, J. Kuper and B. Van Houten, Prokaryotic nucleotide excision repair, *Cold Spring Harbor Perspect. Biol.*, 2013, **5**(3), a012591.

45 S. L. Lusetti and M. M. Cox, The bacterial RecA protein and the recombinational DNA repair of stalled replication forks, *Annu. Rev. Biochem.*, 2002, **71**(1), 71–100.

46 J. Cadet and T. Douki, Formation of UV-induced DNA damage contributing to skin cancer development, *Photochem. Photobiol. Sci.*, 2018, DOI: 10.1039/c7pp00395a.

47 T. Douki and J. Cadet, Individual determination of the yield of the main UV-induced dimeric pyrimidine photoproducts in DNA suggests a high mutagenicity of CC photolesions, *Biochemistry*, 2001, **40**(8), 2495–2501.

48 T. Douki, Low ionic strength reduces cytosine photoreactivity in UVC-irradiated isolated DNA, *Photochem. Photobiol. Sci.*, 2006, **5**(11), 1045–1051.
49 A. V. Tataurov, Y. You and R. Owczarzy, Predicting ultraviolet spectrum of single stranded and double stranded deoxyribonucleic acids, *Biophys. Chem.*, 2008, **133**(1), 66–70.
50 T. Döuki, S. Sauvaigo, F. Odin and J. Cadet, Formation of the main UV-induced thymine dimeric lesions within isolated and cellular DNA as measured by high performance liquid chromatography-tandem mass spectrometry, *J. Biol. Chem.*, 2000, **275**(16), 11678–11685.
51 M. H. Patrick, Studies on thymine-derived UV photoproducts in DNA-I. Formation and biological role of pyrimidine adducts in DNA, *Photochem. Photobiol.*, 1977, **25**(4), 357–372.
52 J. A. Sikorsky, D. A. Primerano, T. W. Fenger and J. Denvir, Effect of DNA damage on PCR amplification efficiency with the relative threshold cycle method, *Biochem. Biophys. Res. Commun.*, 2004, **323**(3), 823–830.
53 M. Matzeu and G. Onori, Effect of mid-UV radiation on DNA-Cu^{2+} complex: Absorption and circular dichroism study, *Photochem. Photobiol.*, 1986, **44**(1), 59–65.
54 P. Natarajan and J. F. Endicott, Photoredox behavior of transition metal-ethylenediaminetetraacetate complexes. A comparison of some group VII metals, *J. Phys. Chem.*, 1973, **77**(17), 2049–2054.
55 J. Cadet and J. R. Wagner, DNA base damage by reactive oxygen species, oxidizing agents, and UV radiation, *Cold Spring Harbor Perspect. Biol.*, 2013, **5**(2), a012559.
56 A. Maor-Shoshani, V. Ben-Ari and Z. Livneh, Lesion bypass DNA polymerases replicate across non-DNA segments, *Proc. Natl. Acad. Sci. U. S. A.*, 2003, **100**(25), 14760–14765.
57 P. Nevin, C. C. Gabbai and K. J. Marians, Replisome-mediated translesion synthesis by a cellular replicase, *J. Biol. Chem.*, 2017, **292**(33), 13833–13842.